Environmental Sciences Europe

RESEARCH

Open Access

Parametric modelling and analysis to optimize adsorption of Atrazine by MgO/Fe_3O_4-synthesized porous carbons in water environment

Lartey-Young George[1], Limin Ma[1,2*], Weiwei Zhang[1] and Guodong Yao[1]

Abstract

Background Pesticide contamination to water, continues to raise ecotoxicological and human concerns. Studying the application of green adsorbents for removing pesticides from water can significantly reduce ecotoxicological impacts and sustain reclamation of water bodies.

Results The current study investigated the adsorption capacity of MgO/Fe_3O_4 modified coconut shell biochar (MCSB) towards Atrazine removal in water. The prepared adsorbents were structurally constricted and obtained relative amount of mesopore spaces filled by nanoparticles which equally provided active occupancy/binding sites for Atrazine molecule deposition. Equilibrium isotherm studies under temperature regimes of 300 K, 318 K and 328 K were best described by the Freundlich isotherm ($R^2 = 0.95–0.97$) with highest adsorption capacity corresponding to the highest temperature range (328 K) at ($K_F = 9.60$ L mg^{-1}). The kinetics modelling was best fitted to the pseudo second-order kinetic ($R^2 = 0.90–0.98$) reaction pathways revealing that Atrazine uptake and removal occurred majorly over non-homogenous surfaces and high influence of surface functional groups in the process. Atrazine uptake by the adsorbent were mostly efficient within pH ranges of 2–6. Thermodynamics values of free energy $\Delta G°$ were negative ranging ($\Delta G° = -27.50$ to -29.77 kJ mol^{-1}) across the varying reaction temperature indicating an exothermic reaction, while enthalpy ($\Delta H°$) (34.59 kJ mol) and entropy ($\Delta S°$) (90.88 JK^{-1}/mol) values were positive revealing a degree of spontaneity which facilitated Atrazine uptake. The adsorbents regeneration capacities over five cycles were observed to decrease proportionally with maximum yields up to 50–60%. Optimization of the adsorption condition by response surface modelling (RSM) and Central Composite Design (CCD) could reveal optimum conditions for Atrazine removal through interaction of different variables at pH = 12, adsorbate initial concentration at 12 mg L^{-1}, adsorbate dosage at 0.5 g and reaction temperature at 54 °C. The overall mechanisms of the adsorption could be contributed by availability of surface functional groups on the MCSB surface through increase in hydrophilicity facilitating easy Atrazine molecule attachment via hydrogen bonding and improved surface complexation.

Conclusions The as-synthesized MCSB adsorbent could uptake and remove Atrazine in water. A high pH, low concentration, low adsorbent dosage and high reaction temperature could be optimized conditions to attain highest Atrazine removal by the synthesized adsorbent.

Keywords Atrazine, Adsorption, Coconut shell biochar, Response surface methodology

*Correspondence:
Limin Ma
lmma@tongji.edu.cn
Full list of author information is available at the end of the article

Graphical Abstract

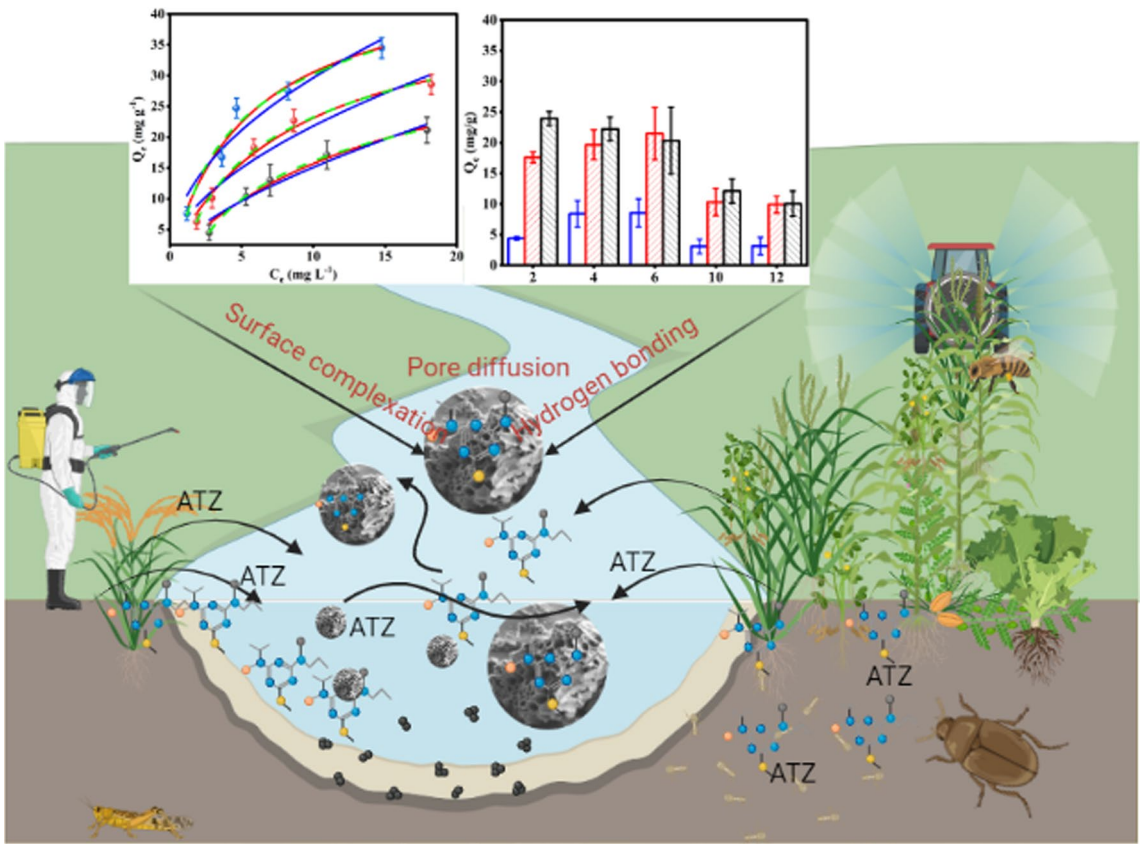

Introduction

Pesticides are ubiquitous contaminants in the environment, since they easily migrate from their source of application to non-target environments [1]. Due to their low detection concentration rates, several approaches have been adopted for their removal but are most limited by cost and potential post remediation contamination effects [2]. However, adsorption is considered a paramount choice due to its easy operation, low cost and fulfillment of the sustainable remediation criteria [3]. Adsorption, however, is reliant on adsorbents. Different ranges of adsorbents have been explored in literature including activated carbon, clay minerals, layered double hydroxides (LDH), metal organic frameworks (MOFs), single- and multi-walled carbon nano tubes (SMWCNT) [4]. Nonetheless, new innovative adsorbents with magnetic properties capable of monitoring and recognizing pollutants are being pioneered [5].

Biochar is progressively drawing global attention as a sustainable environmental remediation agent. This is evidenced in the large research database demonstrating its capacity towards removal of contaminants in freshwater and wastewater [6]. Detailed discussion on biochar preparation and characterization approaches is reported [7–9]. Despite its promising excellence, there is yet drawbacks associated with the application of biochar for removal or treatment of contaminants as some studies have indicated the relatively low adsorption capacities, requirement for longer equilibrium due to lack of functional groups and the difficulty in trapping and treating contaminants hence potential back diffusion of adsorbed contaminants into water [10]. In addition, since original and pristine biochar has low adsorption capacity for anions and electro negative organic molecule [11], it is useful to improve the electronegative organic pollutant (e.g., Atrazine) adsorption capacity on Biochar through modification or functionalization. To improve on biochar's performance, several physicochemical activation

techniques have been investigated [12, 13] and chemical activation is found as efficient; however, this is often challenged based on green chemistry principles, specifically principle 3 'less hazardous synthesis' [14]. Overly synthesized biochar could increase their environmental risk through chemical leaching. A range of chemical reagents commonly applied for biochar enhancement, KOH, NaOH, LiOH, H_2PO_4 is reported [12].

The most proposed effective strategy to resolve this bottleneck through introduction of transition metals and their oxides into the Biochar labyrinth or matrix [15]. Adopting friendly and safe chemical synthesis, therefore, becomes necessary. Transition metals such as (Fe, Co, Ni, among others) or their oxides have recently been introduced into biochar matrices to form magnetic Biochar's [16]. Metal ion intercalation with biochar to form magnetic biochar (MB) is one means to achieve high performing biochar for pesticide removal [17]. By this, biochar possesses magnetic effects which could act like semi-conduits capable of trapping and treating contaminants efficiently. The magnetic effect further makes it feasible for the MBs to be recycled and reused while maintaining their original properties [5]. Previously reported synthesis of MBs for pesticide removal involved the use of single constituents which offered limitations such as reduced pore spaces and volumes to the adsorbent hence limiting their performance [18]. Contrarily, the binary composition of chemical compounds is seen to better efficiently promote MBs performance as demonstrated in the works of Romero et al. who synthesized magnetic covalent organic frameworks (COF's) for removal of endocrine disrupting chemicals in water through surface amino functionalization with $FeCl_3.6H_2O$ and $FeCl_3.4H_2O$ and found higher removal rates for Atrazine [19]. In addition, Nejadshafiee and Islami [20] studied the removal of Acetamiprid by Fe_3O_4 and ascorbic acid-synthesized biosorbents in water and recorded higher removal rates.

Liang et al. [21] also investigated the effect of four Fe/Mn-modified Biochar's to enhance Atrazine removal and found that the formation of oxygen functional groups (OH, C=C, and C=O) could highly facilitate Atrazine removal. Similar observations were reported by Tao et al. [22], through application of Fe modified corn cob Biochar. According to Yang et al. [23], such Atrazine removal process is also facilitated by the introduction of strongly electronegative N atom which can reduce the electron density on the surface of the biochar, thereby increasing the π electron acceptability of the Biochar. Atrazine which is generally considered to be a π-donor due to its π-electron enrichment, resulting in the interaction of π–π electron donor–accepter between Atrazine and the modified Fe biochar to facilitates adsorption. Cao et al. [24], also modified biochar with Fe-phenol to enhance Atrazine removal by ferrate Fe(VI) under alkaline conditions.

Although the environmental performance of magnesium oxide (MgO) has been demonstrated for removal of several nutrients and heavy metals in water [25] their binary and mutual composition with ferromagnetic agents for pesticide removal has not been explored for Atrazine removal in an aqueous media. Hence, to contribute towards filling the gaps, further investigation to improve the adsorption removal of Atrazine by MgO complexation with iron becomes necessary. Such magnetism of biochar adsorbents could efficiently prevent the destructed nanocomposites from damaging the aquatic environment [26]. According to Rufford et al. [27], application of magnesium salts can fasten the process of cellulose and hemicellulose-based carbon materials, limiting tar generation which disrupt and block establishment of sufficient pore spaces. In addition, biochar composites synthesized by MgO have been demonstrated for removal of organic compounds like dyes relying on the high specific surface area formation and enormous active binding site formation [28].

Atrazine (2-chloro-4-ethylamino-6-isopropyl-amino-s-triazine) contamination of water bodies has been reported under several critical conditions due to its low solubility and partial dissolution. Recent studies have indicated very low Atrazine concentrations in water bodies rendering their removal challenging [22]. These concerns have promulgated revisions in water quality indices and in countries, such as China, the minimum detection limits (MDL) are set at 3.0 μg L^{-1} for surface water and 2.0 μg L^{-1} drinking water supply [29]. Hence, the prime objective from this investigation was to study the performance of MgO/Fe_3O_4 synthesized on coconut shell biochar composites for Atrazine removal in water. Such combination may be of immense interest establishing new properties and possible better performance of for Atrazine removal relying on the magnetic capacities of the adsorbents. We explored the independent process variables, i.e., Atrazine initial concentration, pH, contact time, adsorbent dosage and temperature on the overall efficiency for Atrazine removal. To capture the intrinsic features of the adsorbent, interaction within the different process variables and minimized experimental stages, response surface methodology (RSM) is employed to estimate optimum conditions for Atrazine removal [30]. To reveal the mechanism involved in the adsorption process, two parameter non-linear isotherm and kinetic models are applied. For practical application, coconut shell biochar (CSB) used. CSB has high microstructure, high carbon, oxygen and hydrogen content which some studies have demonstrated their strong affinities for

contaminants, such as heavy metals [31] and nutrients [32]; however, there is paucity of data on CSB towards pesticides removal in aqueous environments [33–35] which further resonates the findings in this study.

Materials and methods

Chemicals and reagents

Pure grade Atrazine standard 99% (Dr. Ehrenstorfer, Augsburg-Germany) was purchased from Tansoole Co. Ltd (Shanghai, China P.R) and used for all experiments and analytical measurement. Some characteristics of Atrazine is shown in Additional file 1: Table S1. Biochar was sourced from local market in (Shanghai, China, P.R). Magnesium chloride hexahydrate ($MgCl_2.6H_2O$) and Iron chloride (III) hexahydrate ($FeCl_3.6H_2O$) were purchased from Tansoole Company Ltd (Shanghai, China P.R) and particle size sieves with mesh No. 10 corresponding to 2 mm particle size from Sinopharm Chemical Reagent Co. Ltd (Shanghai, China P.R).

Adsorbent synthesis

Coconut shell biochar (CSB) was soaked and washed in ultrapure water (Milli-Q Advantage A10 system, resistivity = 18.2 $M\Omega cm^{-1}$) for 60 min followed by sitting in an ultrasound bath (GT Sonic D6, 40 kHz, 300 W heating power) for 30 min to remove any impurities, thereafter oven-dried at 105 °C for 8 h. To synthesize the CSB MgO/Fe_3O_4 composites, as shown in Fig. 1, 50 g of $FeCl_3.6H_2O$ and 30 g of $MgCl_2.6H_2O$ (w/w) were added to a 1000 ml beaker and stirred until solid mixture of the two chemical agents/precursors were obtained. 150 mL of deionized (DI) water was added while gently stirring until a uniform solution of the solids were obtained. 30 g of the cleaned CSB was added to the solution of precursors and kept on a magnetic stirrer overnight. The formed chemical composition was separated from solution by a magnet as the aqueous component was decanted. The solid formed MgO/Fe_3O_4 biochar composites were double washed in deionized water until the pH was near neutral followed by drying at 400 °C for 60 min in a box furnace (MTI KSL 1200XL) then cooled overnight. The formed products were then ground and sieved by sieve/mesh No. 10 (particle size 2 mm) to obtain desired particle size and labeled as MCSB.

Analytical characterization

The adsorbent morphologies and structural arrangements were observed by scanning electron microscope (Phenom G2 Pro Desktop SEM) and further image processing in ImageJ v1.53e [36]. Fourier-transform infrared (FTIR) spectrometer (Nicolet 57000, ThermoFisher Scientific) was used to determine the surface chemical properties in the range of 4000–500 cm^{-1} wavenumber, while XRD analysis performed by (D-8 Advance X Ray Powder Diffractometer, Cu, Kα radiation, 40 kVA, 40 mA, 0.1 step size, 1 s measurement interval) and further results processing of chromatograms in MDI Jade v6.5 (www.materialsdata.com). Zeta potential (pH_{pzc}) was determined following previously described approach by [37]. N_2 adsorption–desorption approach was used to characterize available size and pore volumes (Micromeritics Instrument Corporation, ASAP 2460).

Adsorption studies

Batch adsorption experiments were performed using 50 mL of 5, 10, 15, 20 and 30 mg L^{-1} of Atrazine working solution in an Erlenmeyer flask. 20 mg MB200 adsorbents was added to each flask. The experimental set ups were kept on a thermostatic shaker at 150 rpm at varying temperatures of 303 K, 318 K, and 328 K over 24 h to study the adsorption isotherms. To determine the rate of Atrazine removal, kinetic studies were

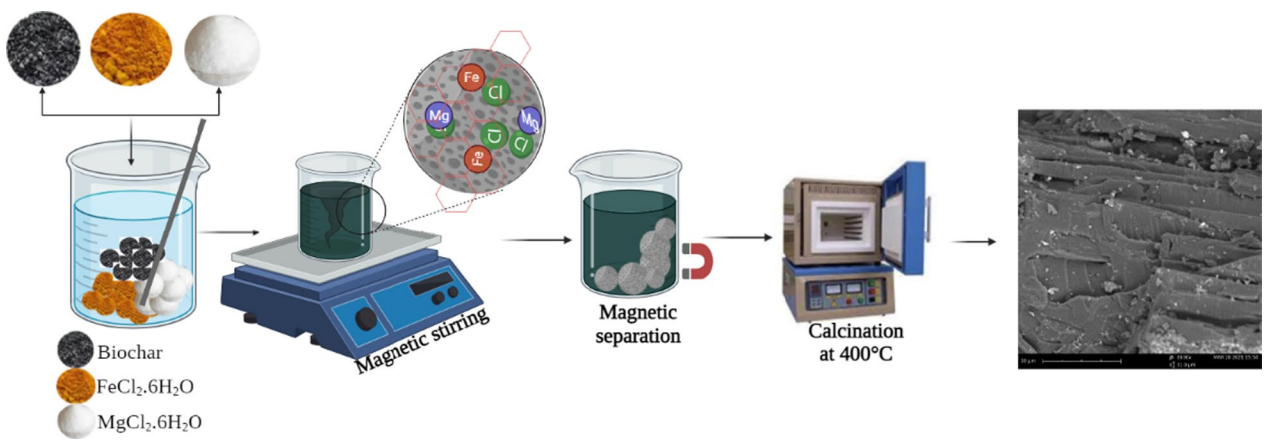

Fig. 1 Facile synthesis of MgO/Fe_3O_4 CSB adsorbents

performed at 318 K at specific time intervals, 0.5 h, 1 h, 3 h, 5 h, 8 h, 12 h, 16 h, by recovering samples and the solid–liquid phase separated by filtration using 0.22 µm pall filters to determine the final analyte concentration. All experiments were performed in triplicate. Independent adsorption studies to determine the effect of pH on the adsorption of Atrazine was experimented with intermediate solutions of 5 mg L^{-1}, 15 mg L^{-1} and 30 mg L^{-1}. The background solution was adjusted using 0.1 M Hydrochloric acid (HCl) and 0.5 M Sodium Hydroxide (NaOH) solution to obtain pH solutions in ranges of 2, 4, 6, 10 and 12.

Experimental design by response surface methodology (RSM)

Response surface methodology (RSM) and Central composite design (CCD) as a powerful tool was employed to optimize the adsorption capacity of the prepared adsorbent. To initiate the process, four parameters in Table 1, i.e., Atrazine concentration (mg L^{-1}), adsorbent dosage (g), pH and reaction temperature (°C) were investigated. The results of 40 independent experimental runs was used to analyze the mathematical relationship between the response (y) and a set of independent parameters (x) following Eq. (1):

$$y = f(x) = \beta_o + \sum_{i=1}^{k} \beta_i X_i + \sum_{i=1}^{k} \sum_{j=1}^{k} \beta_{ij} X_i X_j + \sum_{i=1}^{k} \beta_{ii} X_i^2 \quad (1)$$

where y is the predicted response; x_i and x_j are the independent variables (i, $j = 1, 2, 3, 4, \ldots k$). The parameter β_o is the model constant; β_i is the linear coefficient; β_{ii} is the second-order coefficient and β_{ij} is the interaction coefficient.

Analytical concentration measurement

Analytical measurement of final filtrate was performed using high-pressure liquid chromatography (HPLC-Shimadzu, LC-2030 3D Plus). Peak detection was by an isocratic elution of methanol/water (70:30, v/v) mobile phases, flow rate of 0.8 mL min^{-1}, oven temperature at 30 °C, UV absorbance and pressure at 225 nm, and 20 mpa, respectively. The equilibrium adsorption and removal capacities (q_e, q_t mg g^{-1} and r %), respectively, were determined by mass difference between the initial (C_0) and equilibrium concentration (C_e) following Eqs. (1–3) in Additional file 1: Table S2.

Table 1 List of independent variables and levels

Factor	Unit	Code	Levels	
			− 1	1
Concentration	mg L^{-1}	X_1	5	30
pH		X_2	2	12
Adsorbent dosage	g	X_3	0.5	3
Reaction temperature	℃	X_4	30	55

Results and discussion

Characterization of as prepared adsorbents

Figure 2 shows the SEM images of the as prepared adsorbents. SEM analysis was used to determine the structural and morphological surface changes of the samples. It is seen that the deposition of the Fe_3O_4 particles could have resulted in the surfaces of the natural MCSB to be highly constricted (Fig. 2a). In addition, the MgO/Fe_3O_4 promoted formation of a layered structure which can serve as bridges between MCSB and Fe nanoparticles for adsorption of Atrazine molecules (Fig. 2b). The MCSB also obtained some amount of porosity and roughness which contributes to amount of active binding sites for adsorption. It can be concluded that the MgO/Fe_3O_4 nanoparticles can have a good and effective interaction with the MCSB.

Surface characteristics of the synthesized MCSB is shown in Fig. 3. The XRD pattern for adsorbent is shown in Fig. 3a. The broad peaks were within $2\theta = 20°–30°$ ranges. The peaks at, respectively, 23.18, 33.15, 39.05, 47.25, 49.25, 57.43, 69.67, 83.08 were indexed at 021, 121, 040, 241, 151, 242, 442. The corresponding pair diffraction factor (PDF) which could reveal the efficiency of the synthesis process were assigned to peaks at 23.18° and 83.08° for iron oxide, Fe_2O_3 (PDF No. 73-2234) formation, while peaks at (231.8°, 021), (47.25°, 241) corresponded to MgO formation (PDF No. 72-1609). FTIR spectrum of surface functional groups are shown in Fig. 3b and compared to Sigma-Aldrich Library of FT-R Spectra. The peaks at 3392 cm^{-1} was assigned to O–H stretching vibrations in hydroxyl groups. The peak at 1654 cm^{-1} were assigned to C=C stretching of alkene groups and the peaks at 1558 cm^{-1} was assigned to C=C stretching groups, while the peaks at 1448 cm^{-1} were corresponded to C–H bending vibrations. The peak nodes at 1137 was assigned to C–O stretching vibrations and the weak nodes at 603 cm^{-1} was corresponded to C–L stretching of halo compound formation. The surface $pH_{(pzc)}$ of the adsorbent was determined at 6.3 in Fig. 3c. Some porosity was observed which represented mesopore–macropore formations which could be related to (1). nanoparticles occupying available pore space and, (2). evolution of Mg during calcination which resulted in the collapse of most pore walls, Fig. 3d.

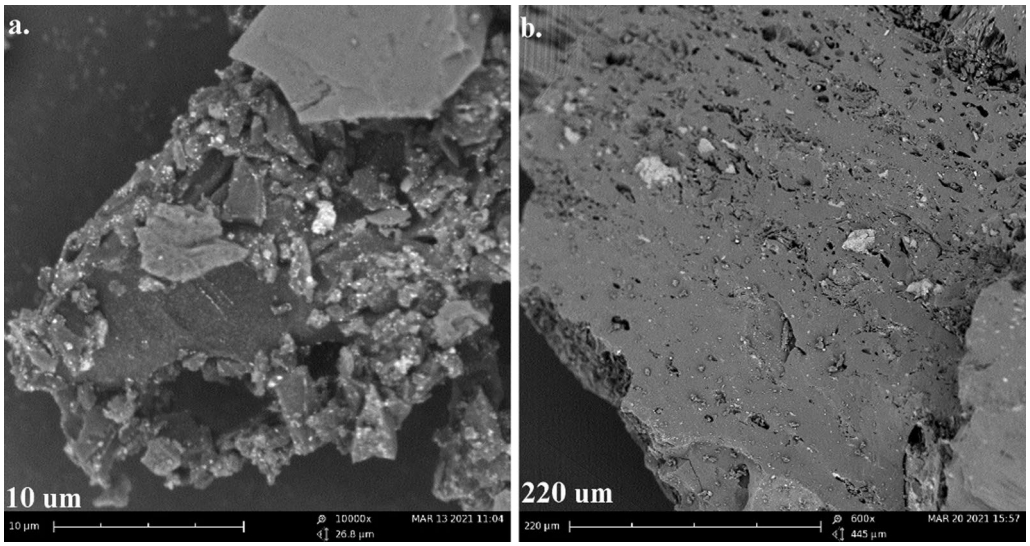

Fig. 2 Morphological arrangements of MCSB

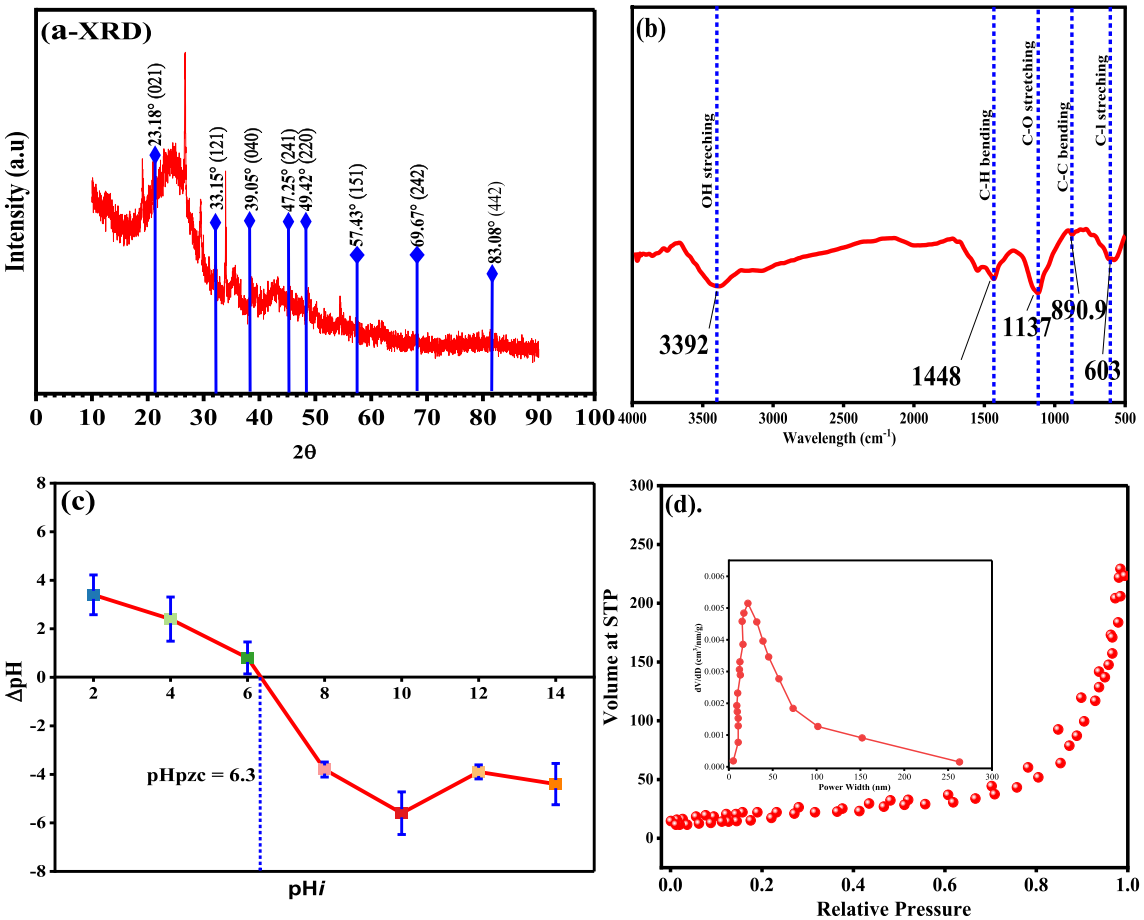

Fig. 3 **a** XRD pattern, **b** FTIR spectra, **c** surface pH of adsorbent (**d**) pore-particle size distribution

Equilibrium adsorption isotherms and kinetics study

Adsorption isotherms and kinetics were established following equations, Eqs. (4–10), in Additional file 1: Table S3. Adsorption isotherms were fitted to the Langmuir, Freundlich and Temkin isotherms in Fig. 4a and Additional file 1: Table S3 describes the adsorption isotherm equilibrium constants. The Langmuir isotherm is established on the assumption that Atrazine molecules become chemically adsorbed on a specific and fixed number of established sites on a homogenous plane. The Freundlich isotherm assumes that Atrazine adsorption will occur on a multilayer process on a heterogenous surface and considers that the molecular binding on the surface of the adsorbents could influence adjacent sites. The Temkin model on the other hand considers that interaction between adsorbent and adsorbate in which it ignores any extremely large and low concentration values. It further assumes that adsorption heats of exchange (ΔH_{ads}) is a function of temperature of all molecules existing in the surface layer declines linearly rather than logarithmically due to increase in surface coverage [38].

Based on the fitting correlation coefficient (R^2), the Freundlich isotherm model could best describe the data sets ranging with ($R^2 = 0.94–0.98$). The association between the data fitting could be associated with heterogenous surface formation contributed by deposition of MgO/Fe_3O_4 nanoparticles which formed large number of active/binding sites for Atrazine molecules in the reaction system. The 1/n values obtained determined were lower than 1 ($1/n < 1$) (0.489–0.651) which confirmed a normal uptake reaction of the Atrazine molecules by the adsorbents and the influence of chemisorption in the adsorption process [39]. The Langmuir isotherm was less favourable ($R^2 = 0.90–0.93$) to the data sets further revealing that Atrazine adsorption occurred through a multi-complex process [40]. Nonetheless, some monolayer layers on the adsorbents surface possibly caused by wall flattening during thermal activation could have

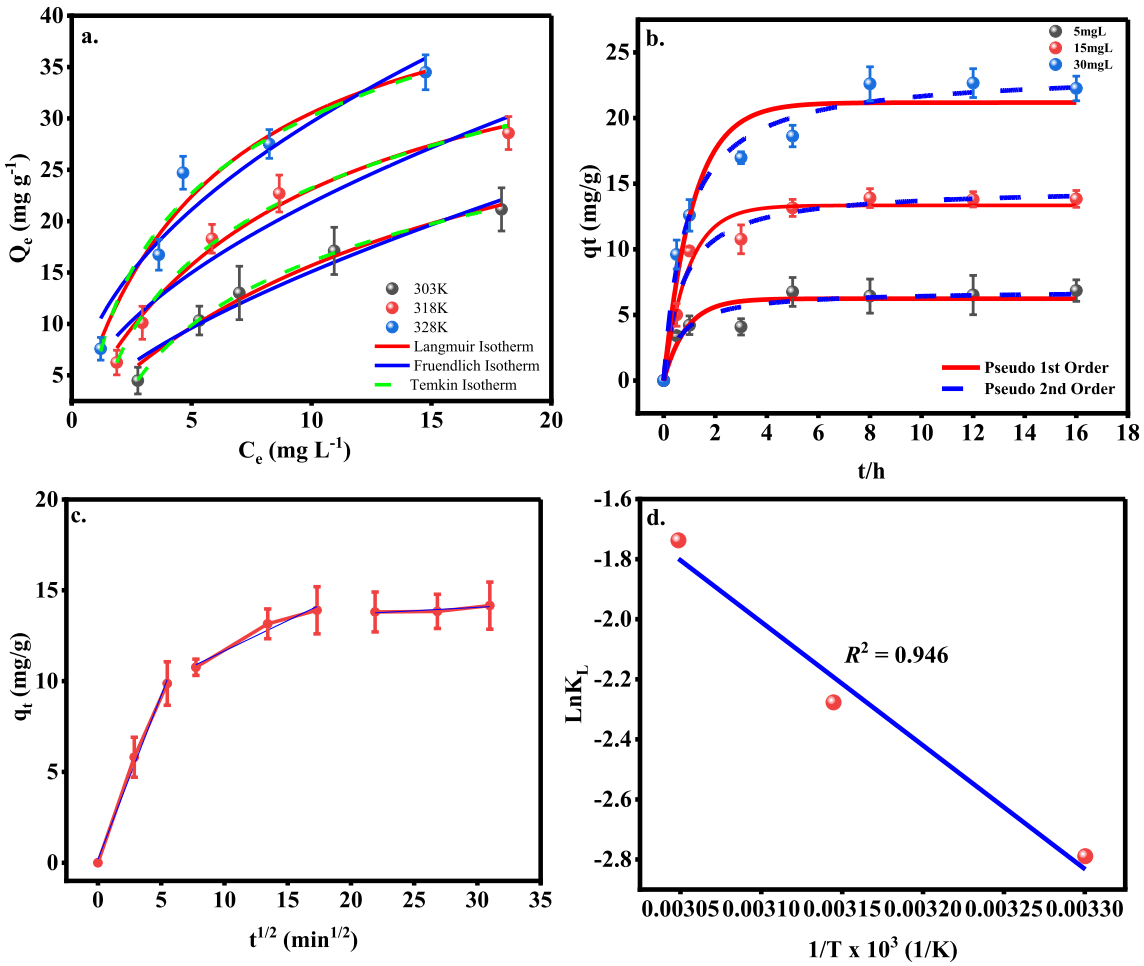

Fig. 4 **a** Adsorption isotherms. **b** Adsorption kinetics. **c** Morris Webber plot of intraparticle diffusion. **d** Thermodynamics plot of LnK_L versus 1/*T*

contributed to the overall adsorption process. The adsorbent separation factor (R_L) was determined as ($R_L < 1$) indicating a favourable reaction process.

An important parameter for adsorbent design for pesticide removal is saturation of adsorption time. The different adsorption equilibrium times plus other factors, pore volumes, pH, adsorbent dosage tend to determine the adsorption rate. The effects of contact time on Atrazine removal is described in Fig. 4b. At the beginning of the adsorption, the mass concentration of Atrazine was higher in solution and there were possible high amount of adsorption sites available on the different sized adsorbents. This is observed by the fast uptake from 0.5 to the 3rd h before establishing equilibrium at after the 5.5th h and beyond. At this point in the process, the adsorption sites were limited by saturation hence gradually decreased. This could be attributed to high driving force and the rapid transfer of Atrazine cations to occupancy binding sites on the adsorbents established by the high agglomeration effect of MgO/Fe_3O_4. Similar results observed by [41].

The fitted kinetic parameters are summarized in Additional file 1: Table S4. Specifically, the pseudo-second-order kinetic model (PSO) R^2 values were in the range of ($R^2 = 0.908–0.981$). Per the R^2 co-efficient values of the models, it was observed that the data sets for both adsorbents underwent a chemiosorption behaviour per PSO indicating the potential role of electron transfer, surface complexation and other interaction species sharing between the adsorbent and Atrazine as dominant factors in removal process [42].

Intraparticle diffusion

The contribution of intraparticle diffusion to the uptake and removal of Atrazine by the porous carbons were further investigated by the linear form of the intraparticle diffusion model (IPD) and represented in Fig. 4c with corresponding co-efficient in Additional file 1: Table S5.

According to Wu et al. [43], K_{id} values can reflect the extent of contribution by initial sorption and intraparticle diffusion to the total sorption process. The first step obtained the most excellent linearization ($R^2 = 0.989$) with corresponding first intraparticle rate constants (K_{id1}) (1.8009 mg/(g/min$^{1/2}$)) indicating the most rapid process, which could be due to film diffusion, whereby a hydrodynamic boundary layer is possibly formed due to diffusion of Atrazine molecules from solution onto the external surfaces of the MCSB. In contrast, the second and final steps witnessed a downward depletion in the second intraparticle rate constant (K_{id2}) (0.33474 mg/(g/min$^{1/2}$)) and third intraparticle rate constant (K_{id3}) (0.03747 mg/(g/min$^{1/2}$)) with corresponding lower R^2 values ($R^2 = 0.931$ and 0.559) from the Webber–Morris equation. The reduction in the adsorption rate order (K_{id}) from $K_{id1} > K_{id2} > K_{id3}$ can be due to resistance of mass transfer which occurs in the second phase [44]. The second step designates the process, where the movement of Atrazine molecules could migrate from the external surfaces of the MCSB to the internal pore regions. The rate limiting step could be determined by the non-zero intercept calculated from the intercept (C) of the second region of the plot. Across the respective investigations, the intercepts of (C) calculated of the plots were greater than zero, which suggested that the process showed a slowed intraparticle diffusion mainly due to small concentration of Atrazine remaining in the aqueous media and saturation of remaining pore spaces by Atrazine molecules [45].

Adsorption thermodynamics

In general, temperature of adsorption impacts the potential of adsorbents towards contaminant uptake and removal by revealing internal mechanisms caused by interactive molecules in gaining or liberating energies. Per Gibbs Free Energy (ΔG°) the effect of temperature conditions is displayed in Fig. 4d and corresponding fitting values in Additional file 1: Table S6. The R^2 values was ($R^2 = 0.946$) indicating a good fit for the data. The values of (ΔG^{o}) were negative (−ve) across the differing temperature regimes revealing an exothermic condition for Atrazine movement onto the adsorbents. The positive ($\Delta H^{o} = 34.59$ kJ/mol) and ($\Delta S^{o} = 90.88$ JK^{-1}/mol) values, however, revealed an endothermic process with corresponding increasing randomness in the reaction system which plausibly resulted in structural changes of the adsorbent and their interactions with the adsorbate further facilitating uptake by the heterogenous surfaces. It is reported in some studies that chemiosorption processes occur when enthalpy values are approximately ($\Delta H^{o} > 40$ kJ mol^{-1}) [46]. However, in this study, the ΔH^{o} was less which could be associated with the fact that Atrazine uptake was substituted in the adsorption mechanism by protons present in oxygen functional groups and electrostatic interactions with delocalized π electrons of aromatic rings [47]. Similar observations were reported by [48]. Furthermore, the ΔG^{o} values could reveal differing amount of energies exerted to establish an equilibrium state of the reactants and the products.

Effect of pH on adsorption

Solution pH can alter the removal of pesticides to and from adsorbents through a continuous change in the amount of charges and the alternate change characteristics which affect dominant adsorption mechanisms

[49]. The results from the study indicated that Atrazine adsorption decreased with corresponding increase in pH for the adsorbents illustrated in Fig. 5a. Considering the surface properties of the adsorbents to the varying solution ranges of pH values, there were possible protonation of surface functional oxygen groups, at higher pH ranges which potentially induced electrostatic repulsion between adsorbents and Atrazine. This possibly suppressed and limited the uptake process. This repulsive effect at high pH ranges could be associated with their lower performance revealing that Atrazine and the MCSB could largely be driven by other significant and prominent mechanisms other than electrostatic forces. These observations were similar to [50]. Possible electrostatic attraction between the adsorbents and adsorbate molecules could predict to be the main factors lead to formation of an external field to enable Atrazine attraction and bonding to the adsorbent. The observations indicate that, higher pH influences lower adsorption of Atrazine onto the adsorbents. Ionic exchanges on the other hand could be illustrative to describe as one of plausible drivers for the adsorbate uptake by the MCSB. Furthermore, π–π EDA, cation–π bonding and H-bonding could be representative forces driving Atrazine uptake at relatively low pH ranges. Hence, the investigation could conclude best pH for efficient for Atrazine adsorption by the MCSB to be in the ranges of 2–6.

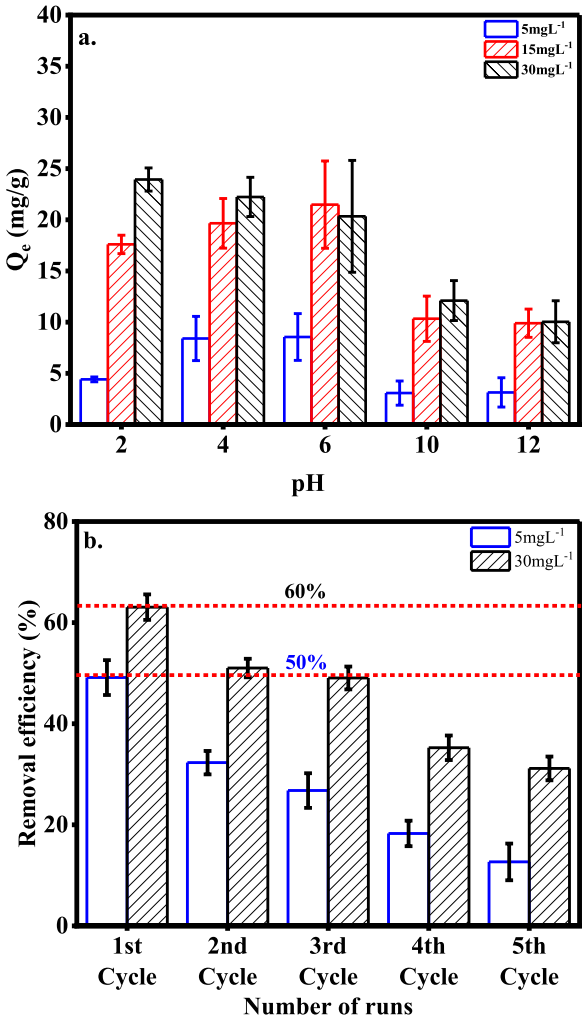

Fig. 5 **a** Effect of pH on adsorption. **b** Regeneration adsorption performance of MCSB

Regeneration and reusability

The methods of regeneration of porous carbon adsorbents have been described [51]. While solvent regeneration is found as an efficient approach amongst others, it was considered as a limitation in this study due to earlier chemical synthesis of the adsorbents further becoming less favourable per 'principle 3' of green chemistry principles [52]. Low temperature thermal regeneration of activated carbons was, however, proposed [53] as an effective means, therefore, a quasi-thermal regeneration process by heating the saturated adsorbents at mild temperature of 100 °C under inert conditions to regain the solids was performed. Regeneration experiments were further performed with initial adsorbate solutions at 5 mg L^{-1} and 30 mg L^{-1} and adsorbent dosage at 15 mg over 24 h. The uptake recoveries were recorded as percentage of mass differences ($C_o - C_e$) over five (5) cycles, as shown in Fig. 5b. Overall, the re-adsorptive capacities of the adsorbents were observed to decrease after the first run from 50% to 60%. As obvious, the nanocomposite effects after initial adsorption runs would have been lost. The mild heating temperature plausibly resulted in re-activation of previously blocked pore spaces hence promotion of significant physisorption in the processes [54].

Results of RSM (central composite design)

Knowledge of the best conditions which can be adjusted to removal Atrazine is important if a large-scale treatment system is to be implemented. The importance of four parameters on removal of Atrazine by the prepared adsorbents was investigated over 40 runs in Design Expert 13. RSM modelling combined with Central Composite Design (CCD) could diagnose the interaction between the variables to affecting Atrazine adsorption. Table 2 shows the actual and predicted values. The second-order polynomial was used to describe the relationship between the variables (x_1, x_2, x_3 and x_4) and response (y %), which in mathematic form was represented as Eq. (3).

Table 2 Matrix of observed and predicted values

Run order	X_1	X_2	X_3	X_4	O	P	Run order	X_1	X_2	X_3	X_4	O	P
1	30	12	0.5	30	24.1	36.79	21	17.5	7	1.75	42.5	68.2	59.41
2	30	2	3	55	43.8	32.93	22	30	2	3	30	84.5	89.09
3	5	2	3	30	72.2	62.32	23	5	2	0.5	55	16.9	31.15
4	17.5	7	1.75	42.5	64.9	59.41	24	5	2	3	55	12.7	5.34
5	17.5	7	1.75	42.5	73.9	59.41	25	30	2	0.5	30	70.6	70.28
6	17.5	7	1.75	42.5	39.2	59.41	26	5	12	0.5	30	51.4	55.17
7	5	12	0.5	55	98.9	88.96	27	17.5	7	4.25	42.5	63.1	76.31
8	17.5	7	1.75	42.5	21.1	59.41	28	17.5	7	1.75	42.5	63.7	59.41
9	42.5	7	1.75	42.5	51.4	53.43	29	5	2	0.5	30	76.9	59.16
10	30	2	0.5	55	70.2	53.78	30	17.5	7	1.75	42.5	19.3	59.41
11	17.5	7	1.75	17.5	59.5	61.86	31	17.5	17	1.75	42.5	86.3	77.76
12	17.5	7	1.75	42.5	85.4	59.41	32	− 7.5	7	1.75	42.5	23.1	33.53
13	17.5	7	1.75	42.5	84.2	59.41	33	17.5	7	1.75	42.5	43.6	59.41
14	17.5	7	1.75	42.5	66.2	59.41	34	17.5	7	1.75	42.5	70.8	59.41
15	17.5	− 3	1.75	42.5	20.5	41.49	35	30	12	3	55	60.8	73.19
16	17.5	7	1.75	67.5	29.4	39.49	36	17.5	7	1.75	42.5	46.3	59.41
17	5	12	3	30	59.2	70.28	37	30	12	0.5	55	79.3	82.08
18	17.5	7	1.75	42.5	67.8	59.41	38	17.5	7	1.75	42.5	61.7	59.41
19	5	12	3	55	71.2	64.42	39	30	12	3	30	88.9	67.55
20	17.5	7	− 0.75	42.5	82.8	82.04	40	17.5	7	1.75	42.5	74.2	59.41

O—Observed, P—Predicted

$$\begin{aligned} y(\%) &= 76.63 + 0.895x_1 + 7.49x_2 - 7.01x_3 + 0.202x_4 \\ &\quad - 0.118x_1x_2 + 0.250x_1x_3 + 0.018x_1x_4 + 0.478x_2x_3 \\ &\quad + 0.247x_2x_4 - 0.634x_3x_4 - 0.025(x_1)^2 \\ &\quad + 0.002(x_2)^2 + 3.16(x_3)^2 - 0.013(x_4)^2. \end{aligned} \tag{3}$$

For additional details, the analysis of variance (ANOVA) was studied to determine whether the quadratic model is sufficient to describe the actual results. To best evaluate the significance level of any proposed model, the modelling parameters including P value (probability), R^2 (coefficient of determination) and AP ratio (adequate precision) should be examined [55]. It is known that the large F test (F value) and the smaller P value are the most significant features to describe a model. At 95% confidence interval, the model can be described as statistically significant if $P < 0.05$, $R^2 \geq 0.9$ and AP > 4. Based on the ANOVA values in Table 3 it is indicative the proposed model was statistically significant, since $P < 0.0397$, and AP = 7.986. The model R^2 value was, however, lower than ($R^2 = 0.64$). In addition, probability (P value) of the lack of fit (LOF = 0.6089) was not significant ($P > 0.05$) revealing the model illustrates a good fit which could navigate the experimental

Table 3 Analysis of variance (ANOVA)

Source	Sum of squares	*df*	Mean Square	*F* value	*P* value
Model	11,592.18	14	828.01	2.22	0.0397[a]
X_1-Conc	594.02	1	594.02	1.59	0.2185[b]
X_2-pH	1972.91	1	1972.91	5.29	0.0301[a]
X_3-Dosage	49.31	1	49.31	0.1322	0.7192[b]
X_4-Temp	750.4	1	750.4	2.01	0.1684[b]
X_1X_2	870.25	1	870.25	2.33	0.1391[b]
X_1X_3	244.92	1	244.92	0.6569	0.4253[b]
X_1X_4	132.25	1	132.25	0.3547	0.5568[b]
X_2X_3	142.8	1	142.8	0.383	0.5416[b]
X_2X_4	3819.24	1	3819.24	10.24	0.0037[a]
X_3X_4	1572.12	1	1572.12	4.22	0.0506[b]
X_1^2	529.68	1	529.68	1.42	0.2445[b]
X_2^2	0.0999	1	0.0999	0.0003	0.9871[b]
X_3^2	815.59	1	815.59	2.19	0.1516[b]
X_4^2	159.1	1	159.1	0.4267	0.5196[b]
Residual	9321.53	25	372.86		
Lack of fit	3318.79	10	331.88	0.8293	0.6089[b]
Pure error	6002.75	15	400.18		
Cor total	20,913.72	39			

[a] Significant (P < 0.05),[b]Non-significant (P > 0.05)

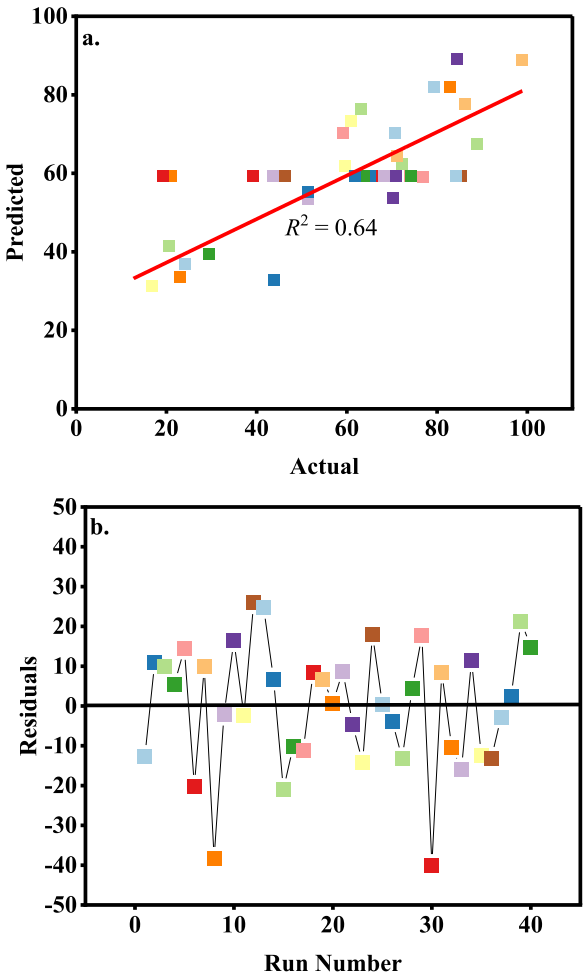

Fig. 6 **a** Plot of predication versus actual and (**b**) residual versus runs

results. In addition, Table 3 can reveal significant interaction effect of involved factors which can results in maximum Atrazine removal. It is observed that, the significant factors were determined to be, pH ($F = 5.29$, $P > 0.05$) as a single factor and interaction of pH and temperature ($F = 0.0037$, $P > 0.05$).

Other signals including 'actual versus predicted' and 'runs versus residual' plots to support compatibility of the such a model is shown in Fig. 6a, b. From Fig. 6a, a relatively good adequacy of the model can be observed based on the distribution of observed versus predicted values on a straight line. Figure 6b shows the plot of residuals against runs which was randomly distributed without patterns. As can be seen in Fig. 7, the perturbation plots enable identification and comparison of all effects of the factors at particular points within the design space. The steep slopes or curvature are indicative that the response obtained in the simulation were sensitive to the factors, while a relatively flat slope describes the insensitivity to change of that specific factor. From Fig. 7, the interaction variables are significant. These were examined according to a three-dimensional space to examine their simultaneous effect on the four parameters based on condition, where other parameters have had consistent and fixed values [56].

To visualize these relationships, a range of three-dimensional plots are shown in Fig. 8. The optimal range of values of parameters to navigate Atrazine removal by the prepared adsorbent is shown in Fig. 9. Although the 3D plots could determine the optimal conditions for the simulated independent parameters, they could be insufficient to predict the optimal conditions. Hence, the independent parameters were optimized to determine the most conditions, where all four factors could be optimized simultaneous to determine the most maximum adsorption capacity of Atrazine by the adsorbent. From Fig. 9, it is observed that the plots of actual profiles of each independent variable in which the optimal points are specified along with the plots of the maximum and minimum yields. The maximum efficiency of the MgO/Fe_3O_4 CSB adsorbents for Atrazine uptake and removal were 93.12% at 30 °C, initial Atrazine concentration at 13.54 mg L^{-1}, adsorbent dosage of 2.9 g and pH at 6.9.

To visualize the adsorption relationships, a range of three-dimensional plots are shown in Fig. 8 and associated contour plots in Additional file 1: Fig. S1. The optimal range of values of parameters to navigate Atrazine removal by the prepared adsorbent is also shown in Fig. 9. Figure 8a shows the effect of interaction reaction of initial Atrazine concentration (X_1) and solution pH (X_2). As observed, the surface of the effects of the independent factors has a peak pH at 10 and a concentration is approximately 25 mg L^{-1}. The maximum predicted removal value based on this interaction was 62%. Similarly, Fig. 8b reveals the interaction of initial concentration (X_1) and adsorbent dosage (X_3). The simulated reaction uptake peak of Atrazine is seen at approximately 27.1 mg L^{-1} and adsorbent dosage of 2.5 g and the maximum removal rate is approximately 75%. Figure 8c shows the reaction interaction of initial concentration (X_1) and temperature (X_4). The surface effects of the parameters are seen at concentration close to 27 mg L^{-1} and the temperature at 46 °C with adsorption removal rate at approximately 58%. Similarly, from Fig. 8d, based on the surface effect, the interaction between pH (X_2) and adsorbent dosage (X_3) of approximately 2 g and pH of 10 was seen as plate-like or with mild slope (i.e., less curvature). This could imply the that Atrazine adsorption yield increased with corresponding increase in adsorbent dosage at the simulated studied conditions. The predicted adsorption removal rate was 78%. Likewise, in Fig. 8e, the surface interaction revealed les curvature, implying that the reaction interaction between pH (X_2) and temperature

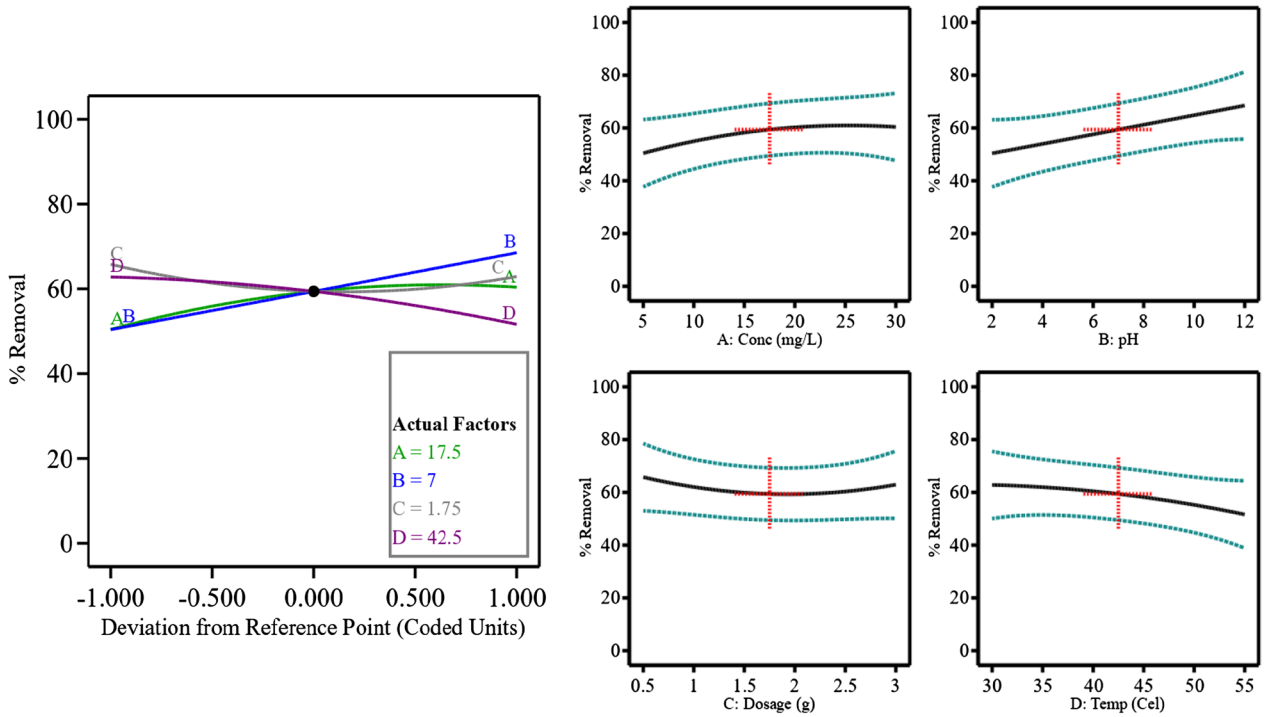

Fig. 7 Perturbation plots of all factors from central point and all factors individually from the central point

(X_4), were proportional and maximum capacities seen at approximately 41.3 °C and pH of 11 with adsorption removal rate at approximately 78%. In Fig. 8f, while the maximum capacities were seen at temperature (X_4) of approximately 30 °C and adsorbent dosage (X_3) of 2.5 g. The predictive adsorption removal rate was approximately 60%.

Possible adsorption mechanism

In general, the adsorption mechanism in this investigation is predicted based on results of the kinetic and isotherm study analysis. The best fit of the pseudo-second kinetics and Temkin isotherm models suggested a significant chemisorption sorption process along the path of Atrazine uptake and removal by the adsorbents. The heterogenous adsorbent surfaces with large active sites formed by nanoparticle deposition could have resulted in interactions between Atrazine and the MgO/Fe_3O_4 contributing to the uptake and removal efficiency in terms of binding to co-similar sites. Co-active sites could also share energies hence it was possible that active sites with higher adsorption energies diffused energies to other active sites with lower in energies. Since both adsorbents did not attain higher surface areas due to constricted surfaces formed by magnetic particles the relatively formed pore spaces could facilitate Atrazine movement hence uptake. Nevertheless, few micro-mesopore volumes were formed with other pore volumes occupied by the nanoparticles.

To evaluate this improvement, the dominant role of MgO and other functional groups in essence were predicted. With most of the pore spaces being occupied, adsorption dependency on active sites were predominant. In addition, since chemisorption was highly predicted from the pseudo-second-order kinetics data, it is anticipated that surface aromatic rings of the Atrazine on the carbon planes and hydrogen bonding interaction between oxygen functional groups on the adsorbent surface occured. Formation of strong Mg–OH bonding was possible during the process mainly due to (1) protonation of MgO by absorbing H^+ from water in the reaction system and acidic condition contributed by nanoparticles and (2) surface ligand complex reaction between the Mg and OH when the reaction solution reaches an alkaline state. In general, the dominant interaction of Atrazine on the surface of the adsorbent could be related to hydrogen bonding interaction between Mg–OH and N atoms Atrazine. The positive trigger of enhanced adsorption capacity included the H-bonding, π–π stacking and electrostatic attraction. The presence of MgO could have further improved the surface properties of adsorbents and provided more active sites in the form of Mg–OH to adsorbed Atrazine leading to the excellent adsorption performance.

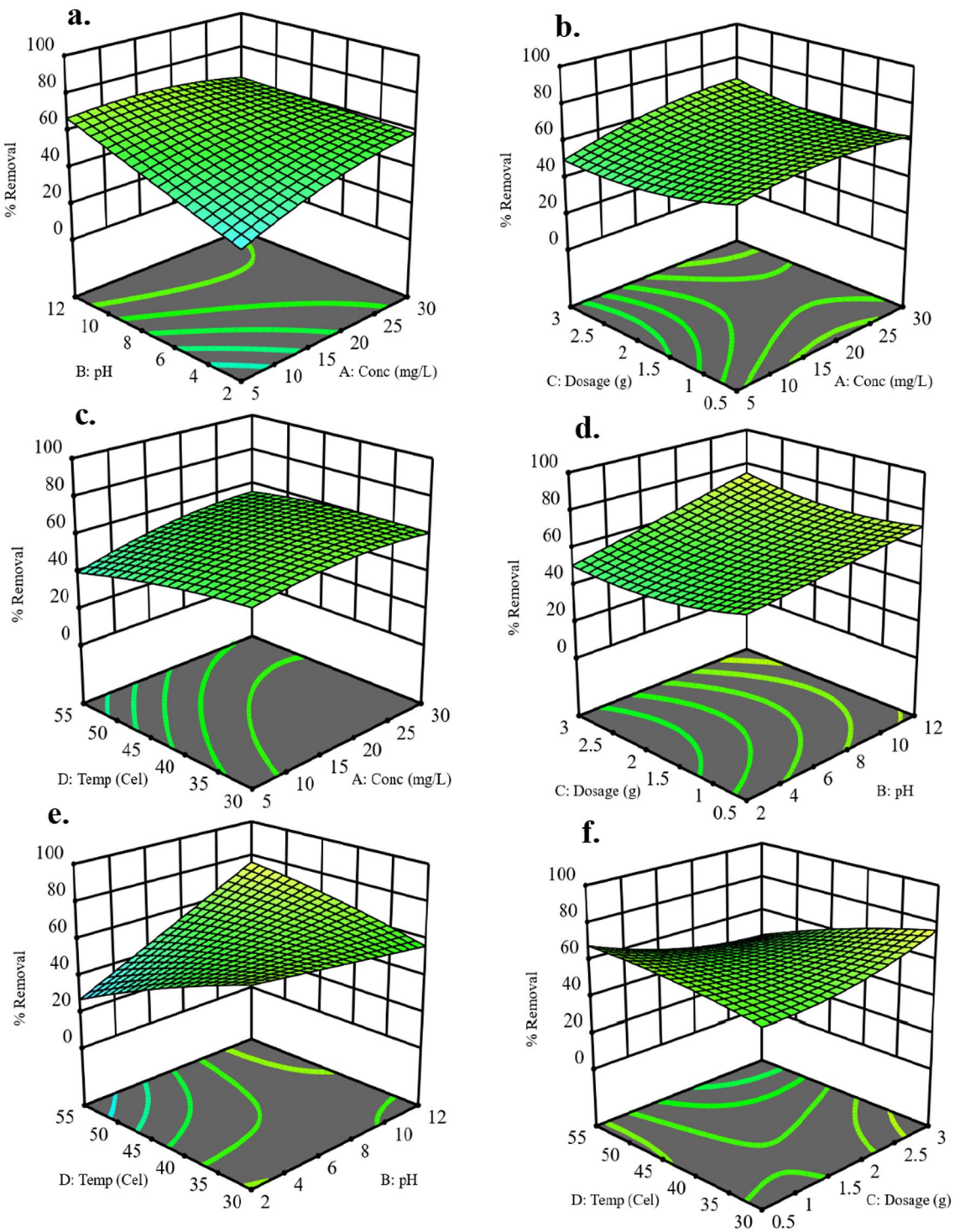

Fig. 8 **a** 3D plots of interaction of (**a**) concentration, pH. **b** Concentration, dosage. **c** Temperature, concentration. **d** Concentration, pH. **e** Temperature, pH; and (**f**) temperature, dosage

Conclusion

In this study, MgO/Fe_3O_4 biochar composites were prepared by low cost fabrication for effective Atrazine removal in an aqueous environment. Overall, the adsorption performance in terms of capacity and efficiency between the adsorbents were comparatively close to

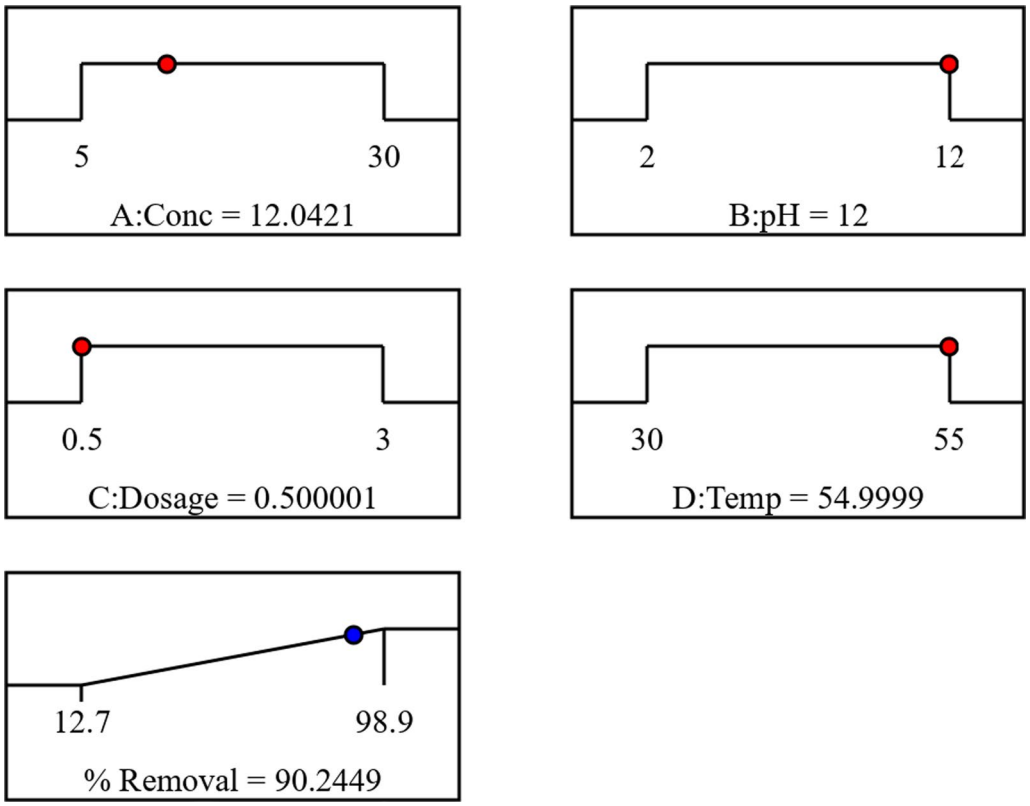

Fig. 9 Actual profiles with predicting points of optimal conditions for Atrazine adsorption

other synthesized adsorbents with maximum adsorption capacities per Langmuir isotherm at 47.80 mg g^{-1}. Atrazine adsorption by the adsorbents reached faster equilibrium and temperature was observed as a dominant factor in the process. Other dominant factors such as surface area, ion exchanges and electrostatic forces were found as highly important for the adsorbents to facilitate Atrazine removal. Overall, the adsorbent characteristics and behaviour was highly influenced by the MgO/Fe_3O_4 formation as demonstrated by adsorption coefficients associated with Freundlich isotherms and pseudo second-order kinetics. The effect of pH further revealed the behaviour of the adsorbents were more efficient at lower pH ranges. An important outcome from this study, is the regeneration approach. Regeneration of the adsorbents after adsorption studies further revealed that, after five (5) recycling runs the spent adsorbents were capable of yielding significant Atrazine removal efficiencies. Optimization studies by CCD and response surface methodology could reveal the results of the experimental studies with best conditions the interaction effect of multiple factors which could yield higher Atrazine removal. Future studies on Atrazine and other typical triazine pesticides should be investigated with this form of synthesized biochar adsorbent. In addition, an exploration of the degradation capacity of MgO/Fe_3O_4 CSB to reveal an understanding of possible transformation products formation is recommended.

Supplementary Information

The online version contains supplementary material available at https://doi.org/10.1186/s12302-023-00725-4.

Additional file 1: Table S1. Characteristics of Atrazine. **Table S2.** List of equations. **Table S3**. Adsorption isotherm constants. **Table S4.** Kinetic parameters of adsorption. **Table S5.** Intra Particle Diffusion Constants of Adsorption. **Table S6**. Thermodynamics Parameters of Adsorption. **Fig. S1.** Contour plots of adsorption prediction (a) Concentration, pH; (b) concentration, dosage; (c) temperature, concentration; (d) concentration, pH; (e) temperature, pH; and (f) temperature, dosage.

Acknowledgements
The authors are grateful to the valuable critique of all reviewers.

Author contributions
GL-Y: conceptualization, investigation, data curation, analysis, writing—original draft preparation; LM: funding acquisition, supervision, validation, resources, writing—review and editing; WZ: data analysis, writing—review and editing, GY: writing—review and editing. All authors read and approved the final manuscript.

Funding
This work was financially supported by Most Key Program of China (2018YFC1803100) and the Natural Science Foundation of China (No. 21377098).

Availability of data and materials
The data sets supporting the conclusions of this article are included within this article.

Declarations

Ethics approval and consent to participate
Not applicable.

Consent for publication
Not applicable.

Competing interests
The authors declare that they have no known competing financial interests or personal relationships that could have appeared to influence the work reported in this paper.

Author details
[1]College of Environmental Science and Engineering, Tongji University, 1239 Siping Road, Shanghai 200092, China. [2]Key Laboratory of Yangtze River Water Environment, Ministry of Education, Tongji University, Shanghai 200092, People's Republic of China.

Received: 4 January 2023 Accepted: 12 March 2023
Published online: 30 March 2023

References

1. Zuanazzi NR, Ghisi ND, Oliveira EC (2020) Analysis of global trends and gaps for studies about 2,4-D herbicide toxicity: a scientometric review. Chemosphere 241:12. https://doi.org/10.1016/j.chemosphere.2019.125016
2. Yeung AT. Remediation technologies for contaminated sites. In: ISGE, editor. International symposium on geo-environmental engineering Hangzhou, China: Springer; 2009. https://doi.org/10.1007/978-3-642-04460-1_25.
3. Hou D, O'Connor D. Green and sustainable remediation: concepts, principles, and pertaining research. In: Hou D, editor. Sustainable remediation of contaminated soil and groundwater. Butterworth-Heinemann; 2020. p. 1–17. https://doi.org/10.1016/B978-0-12-817982-6.00001-X.
4. Ahmad M, Rajapaksha AU, Lim JE, Zhang M, Bolan N, Mohan D et al (2014) Biochar as a sorbent for contaminant management in soil and water: a review. Chemosphere 99:19–33. https://doi.org/10.1016/j.chemosphere.2013.10.071
5. Wang L, Ok YS, Tsang DCW, Alessi DS, Rinklebe J, Wang H et al (2020) New trends in biochar pyrolysis and modification strategies: feedstock, pyrolysis conditions, sustainability concerns and implications for soil amendment. Soil Use Manag 36:358–386. https://doi.org/10.1111/sum.12592
6. Patrick MG, Pan Y, Xiao H, Afzal MT (2019) Progress in preparation and application of modified biochar for improving heavy metal iron removal from wastewater. JBB. 4:21–42. https://doi.org/10.21967/jbb.v4i1.180
7. Kopac T (2021) Hydrogen storage characteristics of bio-based porous carbons of different origin: a comparative review. Int J Energy Res 45(15):20497–20523. https://doi.org/10.1002/er.7130
8. Dai Y, Zhang N, Xing C, Cui Q, Sun Q (2019) The adsorption, regeneration and engineering applications of biochar for removal organic pollutants: a review. Chemosphere 223:12–27. https://doi.org/10.1016/j.chemosphere.2019.01.161
9. Obemah DN, Baowei Z (2014) Biochar preparation, characterization, and adsorptive capacity and Its effect on bioavailability of contaminants: an overview. Adv Mater Sci Eng. https://doi.org/10.1155/2014/715398
10. Ling L-L, Liu W-J, Zhang S, Jiang H (2017) Magnesium oxide embedded nitrogen self-doped biochar composites: fast and high efficiency adsorption of heavy metals in an aqueous solution. Environ Sci Technol 51:10081–10089. https://doi.org/10.1021/acs.est.7b02382
11. Xiang Y, Xu Z, Zhou Y, Wei Y, Long X, He Y et al (2019) A sustainable ferromanganese biochar adsorbent for effective levofloxacin removal from aqueous medium. Chemosphere 237:124464. https://doi.org/10.1016/j.chemosphere.2019.124464
12. Cheng F, Li X (2018) Preparation and application of biochar based catalysts for biofuel production. Catalysts 8:35. https://doi.org/10.3390/catal8090346
13. Lonappan L, Liu Y, Rouissi T, Brar SK, Surampalli RY (2020) Development of biochar-based green functional materials using organic acids for environmental applications. J Clean Prod 244:118841. https://doi.org/10.1016/j.jclepro.2019.118841
14. Liu W-J, Jiang H, Yu H-Q (2015) Development of biochar-based functional materials: toward a sustainable platform carbon material. Chem Rev 115(22):12251–12285. https://doi.org/10.1021/acs.chemrev.5b00195
15. Yi Y, Huang Z, Lu B, Xian J, Tsang EP, Cheng W et al (2020) Magnetic biochar for environmental remediation: a review. Bioresour Technol 298:122468. https://doi.org/10.1016/j.biortech.2019.122468
16. Chen JL, Gao L, Jiang Q, Hou Q, Hong Y, Shen W-J et al (2020) Fabricating efficient porous sorbents to capture organophosphorus pesticide in solution. Microporous Mesoporous Mater 294:109911. https://doi.org/10.1016/j.micromeso.2019.109911
17. Liu L, Wang X, Fang W, Li X, Shan D, Dai Y (2022) Adsorption of metolachlor by a novel magnetic illite biochar and recovery from soil. Environ Res 204:111919. https://doi.org/10.1016/j.envres.2021.111919
18. Mood SH, Ayiania M, Jefferson-Milan Y, Garcia-Perez M (2020) Nitrogen doped char from anaerobically digested fiber for phosphate removal in aqueous solutions. Chemosphere 240:124889. https://doi.org/10.1016/j.chemosphere.2019.124889
19. Romero V, Fernandes SPS, Kovář P, Pšenička M, Kolen'ko YV, Salonen LM et al (2020) Efficient adsorption of endocrine-disrupting pesticides from water with a reusable magnetic covalent organic framework. Microporous Mesoporous Mater 307:110523. https://doi.org/10.1016/j.micromeso.2020.110523
20. Nejadshafiee V, Islami MR (2020) Bioadsorbent from magnetic activated carbon hybrid for removal of dye and pesticide. ChemistrySelect 5(28):8814–8822. https://doi.org/10.1002/slct.202001801
21. Liang Y, Zhao B, Yuan C (2022) Adsorption of atrazine by Fe-Mn-modified biochar: the dominant mechanism of π–π interaction and pore structure. Agronomy 12(12):3097. https://doi.org/10.3390/agronomy12123097
22. Tao Y, Hu SB, Han SY, Shi HT, Yang Y, Li HX et al (2019) Efficient removal of atrazine by iron-modified biochar loaded *Acinetobacter lwoffii* DNS32. Sci Total Environ 682:59–69. https://doi.org/10.1016/j.scitotenv.2019.05.134
23. Yang F, Sun L, Xie W, Jiang Q, Gao Y, Zhang W et al (2017) Nitrogen-functionalization biochars derived from wheat straws via molten salt synthesis: an efficient adsorbent for atrazine removal. Sci Total Environ 607–608:1391–1399. https://doi.org/10.1016/j.scitotenv.2017.07.020
24. Cao Y, Jiang S, Kang X, Zhang H, Zhang Q, Wang L (2021) Enhancing degradation of atrazine by Fe-phenol modified biochar/ferrate(VI) under alkaline conditions: analysis of the mechanism and intermediate products. Chemosphere 285:131399. https://doi.org/10.1016/j.chemosphere.2021.131399
25. Hou L, Liang Q, Wang F (2020) Mechanisms that control the adsorption–desorption behavior of phosphate on magnetite nanoparticles: the role of particle size and surface chemistry characteristics. RSC Adv 10:2378–2388. https://doi.org/10.1039/c9ra08517c
26. Liu H, Mo Z, Li L, Chen F, Wu Q, Qi L (2017) Efficient removal of copper(II) and malachite green from aqueous solution by magnetic magnesium silicate composite. J Chem Eng Data 62(10):3036–3042. https://doi.org/10.1021/acs.jced.7b00041
27. Rufford TE, Hulicova-Jurcakova D, Zhu Z, Lu GQ (2010) A comparative study of chemical treatment by $FeCl_3$, $MgCl_2$, and $ZnCl_2$ on microstructure, surface chemistry, and double-layer capacitance of carbons from waste biomass. J Mater Res 25(8):1451–1459. https://doi.org/10.1557/jmr.2010.0186
28. Zheng X, Huang M, You Y, Fu X, Liu Y, Wen J (2018) One-pot synthesis of sandwich-like MgO@Carbon with enhanced sorption capacity of organic dye. J Chem Eng 334:1399–1409. https://doi.org/10.1016/j.cej.2017.10.156
29. He H, Liu Y, You S, Liu J, Xiao H, Tu Z (2019) A review on recent treatment technology for herbicide atrazine in contaminated environment. Int J Environ 16:5129. https://doi.org/10.3390/ijerph16245129

30. Attallah OA, Wafa MMA, Al-Ghobashy MA, Nebsen M, Monir HH (2021) Adsorptive removal of pesticides from aqueous solutions using chitosan/gelatin polymeric composite: process monitoring and optimization. Int J Environ Sci Technol 19:8183–8194. https://doi.org/10.1007/s13762-021-03694-4
31. Liu H, Xu F, Xie Y, Wang C, Zhang A, Li L et al (2018) Effect of modified coconut shell biochar on availability of heavy metals and biochemical characteristics of soil in multiple heavy metals contaminated soil. Sci Total Environ 645:702–709. https://doi.org/10.1016/j.scitotenv.2018.07.115
32. Zhong Z, Yu G, Mo W, Zhang C, Huang H, Li S et al (2019) Enhanced phosphate sequestration by Fe(iii) modified biochar derived from coconut shell. RSC Adv 9(18):10425–10436. https://doi.org/10.1039/C8RA10400J
33. Baharum NA, Nasir HM, Ishak MY, Isa NM, Hassan MA, Aris AZ (2020) Highly efficient removal of diazinon pesticide from aqueous solutions by using coconut shell modified biochar. Arab J Chem 13:6106–6121. https://doi.org/10.1016/j.arabjc.2020.05.011
34. Kearns JP, Wellborn LS, Summers RS, Knappe DRU (2014) 2,4-D adsorption to biochars: effect of preparation conditions on equilibrium adsorption capacity and comparison with commercial activated carbon literature data. Water Res 62:20–28. https://doi.org/10.1016/j.watres.2014.05.023
35. Yang B, Liu Y, Liang Q, Chen M, Ma L, Li L et al (2019) Evaluation of activated carbon synthesized by one-stage and two-stage co-pyrolysis from sludge and coconut shell. Ecotoxicol Environ Saf 170:722–731. https://doi.org/10.1016/j.ecoenv.2018.11.130
36. Schneider CA, Rasband WS, Eliceiri KW (2012) NIH Image to ImageJ: 25 years of image analysis. Nat Methods 9:671–675. https://doi.org/10.1038/nmeth.2089
37. Noh JS, Schwarz JA (1990) Effect of HNO_3 treatment on the surface acidity of activated carbons. Carbon 28:675–682. https://doi.org/10.1016/0008-6223(90)90069-B
38. Al-Ghouti MA, Da'ana DA (2020) Guidelines for the use and interpretation of adsorption isotherm models: a review. J Hazard Mater 393:122383. https://doi.org/10.1016/j.jhazmat.2020.122383
39. Rajabi M, Keihankhadiv S, Suhas, Tyagi I, Karri RR, Chaudhary M, et al. Comparison and interpretation of isotherm models for the adsorption of dyes, proteins, antibiotics, pesticides and heavy metal ions on different nanomaterials and non-nano materials—a comprehensive review. J Nanostructure Chem. 2022; 13:43. https://doi.org/10.1007/s40097-022-00509-x.
40. Yener J, Kopac T, Dogu G, Dogu T (2008) Dynamic analysis of sorption of methylene blue dye on granular and powdered activated carbon. J Chem Eng 144(3):400–406. https://doi.org/10.1016/j.cej.2008.02.009
41. Chen Y, Shan RF, Sun XY (2020) Adsorption of cadmium by magnesium-modified biochar at different pyrolysis temperatures. BioResources 15(1):767–786. https://doi.org/10.15376/biores.15.1.767-786
42. Magesh N, Renita AA, Siva R, Harirajan N, Santhosh A (2022) Adsorption behavior of fluoroquinolone(ciprofloxacin) using zinc oxide impregnated activated carbon prepared from jack fruit peel: Kinetics and isotherm studies. Chemosphere 290:133227. https://doi.org/10.1016/j.chemosphere.2021.133227
43. Wu F-C, Tseng R-L, Juang R-S (2009) Initial behavior of intraparticle diffusion model used in the description of adsorption kinetics. J Chem Eng 153(1):1–8. https://doi.org/10.1016/j.cej.2009.04.042
44. Mahmoud AED, Fawzy M, Hosny G, Obaid A (2021) Equilibrium, kinetic, and diffusion models of chromium(VI) removal using phragmites australis and ziziphus spina-christi biomass. Int J Environ Sci Technol 18(8):2125–2136. https://doi.org/10.1007/s13762-020-02968-7
45. Tran TV, Nguyen DTC, Le HTN, Vo DVN, Nanda S, Nguyen TD (2020) Optimization, equilibrium, adsorption behavior and role of surface functional groups on graphene oxide-based nanocomposite towards diclofenac drug. J Environ Sci 93:137–150. https://doi.org/10.1016/j.jes.2020.02.007
46. Monárrez-Cordero BE, Sáenz-Trevizo A, Bautista-Carrillo LM, Silva-Vidaurri LG, Miki-Yoshida M, Amézaga-Madrid P (2018) Simultaneous and fast removal of As^{3+}, As^{5+}, Cd^{2+}, Cu^{2+}, Pb^{2+} and F-from water with composite Fe-Ti oxides nanoparticles. J Alloys Compd 757:150–160. https://doi.org/10.1016/j.jallcom.2018.05.013
47. Kuroki A, Hiroto M, Urushihara Y, Horikawa T, Sotowa K-I, Alcántara Avila JR (2019) Adsorption mechanism of metal ions on activated carbon. Adsorption 25:1251–1258. https://doi.org/10.1007/s10450-019-00069-7
48. Diez E, Gomez JM, Rodriguez A, Bernabe I, Saez P, Galan J (2020) A new mesoporous activated carbon as potential adsorbent for effective indium removal from aqueous solutions. Micropor Mesorpor Mat. 295:109984. https://doi.org/10.1016/j.micromeso.2019.109984
49. Herrera-Garcia U, Castillo J, Patino-Ruiz D, Solano R, Herrera A (2019) Activated carbon from yam peels modified with Fe_3O_4 for removal of 2,4-Dichlorophenoxyacetic acid in aqueous solution. Water 11:19. https://doi.org/10.3390/w11112342
50. Xu X, Chen W, Zong S, Ren X, Liu D (2019) Atrazine degradation using Fe_3O_4-sepiolite catalyzed persulfate: reactivity, mechanism and stability. J Hazard Mater 377:62–69. https://doi.org/10.1016/j.jhazmat.2019.05.029
51. Salvador F, Martin-Sanchez N, Sanchez-Hernandez R, Sanchez-Montero MJ, Izquierdo C (2015) Regeneration of carbonaceous adsorbents. Part II: chemical, microbiological and vacuum regeneration. Micropor Mesopor Mat. 202:277–296. https://doi.org/10.1016/j.micromeso.2014.08.019
52. Anastas P (2010) Eghbali NJCSR. Green Chem Principle Pract 39(1):301–312
53. Torrents A, Damera R, Hao OJ (1997) Low-temperature thermal desorption of aromatic compounds from activated carbon. J Hazard Mater 54:141–153. https://doi.org/10.1016/s0304-3894(96)01878-x
54. Zhou Q, Wang W, Shuang C, Wang M, Ma Y, Li A (2014) Reusable magnetic microspheres for efficient removal of atrazine in aqueous media. Chem Eng J 253:190–197. https://doi.org/10.1016/j.cej.2014.05.035
55. Qureshi T, Memon N, Memon SQ, Yavuz H, Lachgar A, Denizli A (2019) Evaluation of hydrocar efficiency for simultaneous removal of diclofenac and ibuprofen from aqueous system using surface response methodology. Environ Sci Pollut Res 26:9796–9804. https://doi.org/10.1007/S11356-019-04359-Z
56. Bezerra MA, Santelli RE, Oliveira EP, Villar LS, Escaleira LA (2008) Response surface methodology (RSM) as a tool for optimization in analytical chemistry. Talanta 76(5):965–977. https://doi.org/10.1016/j.talanta.2008.05.019

Publisher's Note